Learning-based calibration of a high-precision monocular vision system for macro-micro manipulation

Sheng Yao, Xianmin Zhang, and Hai Li

Abstract— **Calibration is critical for the optical vision measurement system (OVMS) that requires high measuring accuracy within a large field of view. In this paper, we propose a practical two-step calibration method that improves measuring accuracy for the multi-scale vision measurement system based on a learning-based approach. In this method, an OVMS combined with a degenerated perspective-n-points algorithm is established for macro-micro manipulation systems. After the OVMS is coarsely calibrated by the analytic technique, the fine calibration is performed using the Artificial Nerual Network to compensate for both geometric and non-geometric measuring errors. Simulations, experiments and comparisons are carried out with a laser tracker, and the results show that the proposed two-step calibration method can remarkably minimize measuring errors and shows stronger robustness and stability, which enables the OVMS to be capable of macro-micro manipulation tasks.**

I. INTRODUCTION

The macro-micro manipulator systems have drawn considerable attention in the field of precision engineering at small scales due to the desirable properties of large-travel, high-precision, and multiple degree-of-freedom (DOF) [1], [2], [3]. The common point of such systems is they all consist of a macro part carrying a micro part. While the macro manipulator provides coarse positioning within a large workspace, the micro part aims to complete the fine positioning and achieve high manipulation accuracy. Therefore, in order to maintain the successful combination of macro-micro manipulators, it is necessary to keep the positioning accuracy of macro part smaller than the workspace of the micro part, which brings up a challenging work to set up a multi-scale measurement method.

Thanks to the properties of non-contact, high resolution and strong expandability, the optical vision measurement system (OVMS) have become a popular selection for multi-DOF measurement in micromanipulation. Although many OVMSs have been adopted in regular robotic applications such as kinematic calibration [4] and grasping tasks [5], it still remains a demanding job to ensure the combination of macro-micro manipulators using OVMSs, which usually requires a measurement system to obtain micro-scale absolute accuracy with a decimeter-scale field of view. It is known that the performance of vision systems is strongly dependent upon calibration. To date, many methods for calibrating OVMS have been presented [6], [7], [8]. However, these conventional methods can hardly achieve required accuracy due to the inaccurate sensor geometry and optical characteristics. Klette *et al.* [9] report that idealized mathematical modeling of lens distortion will lead to an infinite number of distortion coefficients, which will boost the computational cost and is not realistic to calculate. Additionally, practical factors, such as environmental conditions and randomized manufacturing errors, also worsen the measuring accuracy. For example, Su *et al.* [10] observe that pixel shape and size often vary between CCD array location. Thus, errors and uncertainties involved with OVMSs cannot be eliminated but minimized, so that some forms of compensation should be employed.

While analytic techniques can barely handle non-symmetrical and nonlinear errors, learning-based approaches are able to resolve these problems. Modeling the systems from experience data directly, the learning-based techniques are expected to well suited to complex system behaviors, which are hard to be associated with analytical models. Inspired by the information process in the biological neural networks, the Artificial Neural Network (ANN) is an efficient model for statistical pattern recognition, and it gradually becomes the most potential research field in machine learning, which have been broadly applied in many areas of industry [11]. Smith *et al.* [12] employ a scanning laser line and vision system using ANN methods to reduce height measurement error of 3D-objects. Cerveri *et al.* [13] develop two techniques, namely local unwrapping polynomials and RBF ANN, to correct the image distortion of the x-ray. The strong capability to model confounded non-linear data that contains significant noise makes ANN adapted to many image correction tasks.

To the best of our knowledge, few studies have presented a multi-scale machine vision calibration for macro-micro manipulation using ANN. In this paper, we propose a practical and high-accuracy calibration method for OVMSs with the learning-based technique. The system setup of the manipulator platform and geometry model of OVMS are given in details, and a coarse-to-fine calibration strategy that combines an analytic approach and an ANN is developed to minimize the measuring errors of OVMS. To verify the performance of the proposed method, simulations, experiments, and comparisons are carried out.

*This work was supported by the National Natural Science Foundation of China (51820105007, 51905176), and the Fundamental Research Funds for the Central Universities (2019MS057).

Sheng Yao, Xianmin Zhang, and Hai Li are with the Guangdong Key Laboratory of Precision Equipment and Manufacturing Technology, South China university of Technology, Guangzhou 510640, China (E-mail: me syao@mail.scut.edu.cn; zhangxm@scut.edu.cn; lihai@scut.edu.cn)

978-1-7281-9349-6/20/$31.00 ©2020 IEEE

II. METHODOLOGY

A. Setup and Geometric Model of the OVMS

Comparing with the series mechanism structures, parallel mechanisms have the advantages of high stiffness, high accuracy, and high repeatability [14], [15]. Therefore, the planar parallel manipulator (PPM) becomes one of the best candidates in micro-manipulation, and it is selected as the macro part in macro-micro manipulation to provide coarse positioning and load the micro positioner.

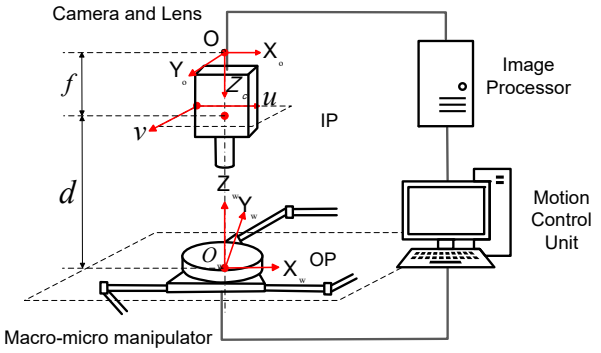

Fig. 1. Configuration of the OVMS for the macro-micro manipulator.

The geometric model of the OVMS is sketched in Fig. 1, where OP denotes the object plane, IP represents the image plane, and O_o is the optical center. f is the focal length, and d is $X_oY_oY_oZ_o$ is the optical sensor coordinate, $X_wY_wZ_w$ is the world coordinate on OP, $\mu\nu$ is the image coordinate on IP, whose origin is located at the top-left corner. Based on the pinhole model [16], the projective transformation equation can be written as

$$\begin{bmatrix}\mu\\ \nu\\ 1\end{bmatrix} = s\boldsymbol{K}\left[\boldsymbol{R},\boldsymbol{T}\right]\begin{bmatrix}x\\ y\\ z\\ 1\end{bmatrix} \tag{1}$$

where s denotes a scale factor, $\boldsymbol{K}$ represents the intrinsic matrix, $\boldsymbol{R}$ is the rotation matrix, and $\boldsymbol{T}$ signifies the translation vector. Since OP and IP are parallel, the independent parameter number in R can be degenerated to one. According to Eq. (1) and Fig. 1, we obtain

$$\begin{bmatrix}\mu\\ \nu\\ 1\end{bmatrix} = s\begin{bmatrix}\alpha & 0 & \mu_0\\ 0 & \beta & \nu_0\\ 0 & 0 & 1\end{bmatrix}\begin{bmatrix}\cos\theta & \sin(\theta+\pi) & 0 & t_x\\ -\sin\theta & \cos(\theta+\pi) & 0 & t_y\\ 0 & 0 & -1 & t_z\end{bmatrix}\begin{bmatrix}X_w\\ Y_w\\ Z_w\\ 1\end{bmatrix} \tag{2}$$

where θ represents the rotation angle between OP and IP coordinates, (μ_0, ν_0) is the principal point, (t_x, t_y, t_z) represents the transnational vector, α is scale factor in μ-coordinate direction, and β is the scale factor in ν-coordinate direction. We name this equation the degenerated perspective-n-points model (DPnP).

From Eq. (2), $s = \frac{1}{t_z}$ can be acquired. Then, we get the following equation

$$\begin{bmatrix}\mu-\mu_0\\ \nu-\nu_0\end{bmatrix} = \begin{bmatrix}\frac{\cos\theta}{t_z}\alpha X_w - \frac{\sin\theta}{t_z}\alpha Y_w + \frac{t_x}{t_z}\alpha\\ -\frac{\sin\theta}{t_z}\beta X_w - \frac{\cos\theta}{t_z}\beta Y_w + \frac{t_y}{t_z}\beta\end{bmatrix} \tag{3}$$

Assuming $a_1 = \frac{t_x}{t_z}, a_2 = \frac{t_y}{t_z}, a_3 = \frac{\sin\theta}{t_z}, a_4 = \frac{\cos\theta}{t_z}$, the non-linearity of Eq. (3) can be removed, and we can construct

$$\begin{bmatrix}\mu-\mu_0\\ \nu-\nu_0\end{bmatrix} = \begin{bmatrix}a_1\alpha - a_3\alpha Y_w + a_4\alpha X_w\\ -a_2\beta - a_3\beta X_w + a_4\beta Y_w\end{bmatrix} \tag{4}$$

To solve Eq. (4), it can be seen that at least two control points are required to bring two constraints, so that the parameters (a_1, a_2, a_3, a_4) can be obtained. If there are n control points, Eq. (4) can be modified into the form

$$\underbrace{\begin{bmatrix}a_1\\ a_2\\ a_3\\ a_4\end{bmatrix}}_{\boldsymbol{a}}\underbrace{\begin{bmatrix}\alpha & 0 & -\alpha Y_1 & \alpha X_1\\ 0 & \beta & -\beta X_1 & -\beta Y_1\\ \vdots & \vdots & \vdots & \vdots\\ \alpha & 0 & -\alpha Y_n & \alpha X_n\\ 0 & \beta & -\beta X_n & -\beta Y_n\end{bmatrix}}_{\boldsymbol{M}} = \underbrace{\begin{bmatrix}\mu_1-\mu_0\\ \nu_1-\nu_0\\ \vdots\\ \mu_n-\mu_0\\ \nu_n-\nu_0\end{bmatrix}}_{\boldsymbol{b}} \tag{5}$$

If $n = 2$ and all the n control points are non-coincidence, vector $\boldsymbol{a}$ can be obtained by $\boldsymbol{a} = A^{-1}\boldsymbol{b}$. Once $n > 2$, Eq. (5) turns into a over-determined linear equation system, and it becomes to find a result $\boldsymbol{a}$ that minimize $\|\boldsymbol{a}\boldsymbol{M} - \boldsymbol{b}\|$. In this case, the normal equation method is employed to seek for a solution that is closest to $\boldsymbol{a}\boldsymbol{M} = \boldsymbol{b}$. In other word, we have the following equations:

$$\begin{cases}\boldsymbol{a} = \boldsymbol{M}^{-1}\boldsymbol{b}, & n = 2\\ \boldsymbol{a} = (\boldsymbol{M}^T\boldsymbol{M})^{-1}\boldsymbol{b}, & n > 2\end{cases} \tag{6}$$

After $\boldsymbol{a}$ is obtained by solving Eq. (6), the values of θ, t_x, t_y, t_z can be calculated.

B. System Calibration

The calibration of vision-based systems aims to determine the model of OVMS and reduce the measuring errors, so that the measured value is as close as possible to the actual value. The proposed calibration method is composed of two steps. The first step is to coarsely calibrate the OVMS with an analytic technique, while the second step is to use a learning-based approach for fine calibration.

According to the DPnP model shown above, the coarse calibration for the OVMS is performed using the method proposed in literature [17], since it is one of the most recognized analytic approaches. Although the physical model parameters are best set by the coarse calibration, there is the residual error that cannot be completely compensated by only changing the parameters. Therefore, ANN is applied to further calibrate the OVMS. The residual error $\boldsymbol{e}$ can be defined as

$$\boldsymbol{e} = \|\boldsymbol{v}_a - \boldsymbol{v}_m\| \tag{7}$$

where $\boldsymbol{v}_m$ is the measured value after the coarse calibration, $\boldsymbol{v}_a$ is the actual value. After that, the minimization problem in the fine calibration can be written as

$$min\|\boldsymbol{v}_a - \boldsymbol{v}_m - \boldsymbol{y}(\boldsymbol{x})\| \tag{8}$$

where $\boldsymbol{x} = [x, y, \theta]$ is the input vector, $\boldsymbol{y}(\boldsymbol{x})$ denotes the ANN model. Once, $\boldsymbol{v}_a$ and $\boldsymbol{v}_m$ are obtained, Eq. (8) can be solved by calculating the ANN model.

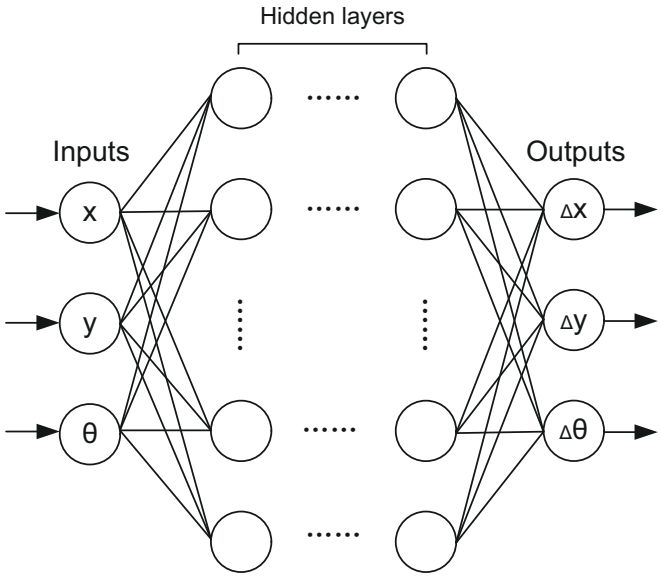

Fig. 2. Schematic of neural networks.

As a supervised learning, the ANN uses parametric forms for the basis functions, where the parameter value will be adjusted during the training process [18]. As can be seen in Fig. 2, the ANN consists of three main part: the input layer, the hidden layers, and the output layer. The inputs in the input layer are the measurement of OVMS $\boldsymbol{x} = [x, y, \theta]$, while outputs in the output layer are the compensation in fine calibration $\boldsymbol{y} = [\Delta x, \Delta y, \Delta\theta]$. Each neuron in hidden layers contains a basis function, which is a nonlinear function of a linear combination of the inputs. Concretely, the linear combinations of hidden layers' inputs I_i can be formulated as

$$a_j = \sum_{i=1}^{n} \omega_{ji}^{l} I_i \tag{9}$$

where $j = 1, ..., m$ is the neuron number of l th hidden layer, n is the input number of l th hidden layer, ω_{ji}^{l} and a_j are defined as weights and activation, respectively. Then, each of these combinations is transformed using a non-linear and differentiable activation function. Compared with the standard tanh activation function [19], Rectified Linear Units (ReLU) [20] shows more biologically plausible and converges much faster. Therefore, in this ANN method, ReLU is employed with the advantages of computational efficiency and non-saturation, which can be written as

$$O_j = max(0, a_j) \tag{10}$$

where O_j is the output of the j th neuron as well as an input in the next layer. Each hidden layer repeats Eqs. (9) and (10) to pass the data to the output layer.

Linking from the input layer to the output layer, the ANN then serves as a parametric non-linear functions from input vector $\boldsymbol{x}$ and the output vector $\boldsymbol{y}$. The is achieved by the network training, where the weights in the hidden layers are tuned according to the training data. Given a training set comprising a set of input vector $\boldsymbol{x_n}$, where $n = 1, ..., N$, and a corresponding set of target vectors $\boldsymbol{t_n}$, we need to minimize the error function:

$$E(\boldsymbol{\omega}) = \frac{1}{2} \sum_{n=1}^{N} \|\boldsymbol{y}(\boldsymbol{x_n}, \boldsymbol{\omega}) - \boldsymbol{t_n}\|^2 \tag{11}$$

where $\boldsymbol{y}(\boldsymbol{x_n}, \boldsymbol{\omega})$ is the output vector of the ANN during training, $\boldsymbol{\omega}$ represents the weight matrix of ANN. Then, our goal turns to find a weight matrix $\boldsymbol{\omega}$ that minimizes the function $E(\boldsymbol{\omega})$. Since $E(\boldsymbol{\omega})$ is a smooth continuous function of $\boldsymbol{\omega}$, the smallest error value will occur when the gradient vanishes as

$$\nabla E(\boldsymbol{\omega}) = 0 \tag{12}$$

In order to compute the gradients of the error function with respect to weights, back-propagation is involved to update the weights in each neuron. According to the chain rule for partial derivative, we construct

$$\frac{\delta E(\boldsymbol{\omega})}{\delta \omega_{ji}} = \frac{\delta E(\boldsymbol{\omega})}{\delta a_j} \frac{\delta a_j}{\delta \omega_{ji}} \tag{13}$$

Then, the weights in each neuron can be obtained. However, there will normally be many inequivalent stationary points and minima for Eq. (12). Since it is unrealistic to find an analytical solution, iterative numerical procedures are resorted. Among many optimization approaches, Limited-memory Broyden-Fletcher-Goldfarb-Shanno (L-BFGS) algorithm is highly competitive with fast convergence rate due to the use of second derivatives of the error $\frac{\delta^2 E(\boldsymbol{\omega})}{\delta \omega_{ji} \delta \omega_{lk}}$, and L-BFGS works much better than other candidates for lower dimensional problems and small datasets [21]. For the OVMS in parallel manipulator system, only a few hundred measurement data at target points will be acquired as training data. Thus, L-BFGS algorithm is applied, and it is expected to converge faster and perform better.

Although a large number of layers in ANN may increase the performance, the model would be over-fitting and suffer a decrease in the accuracy with small training data. A large number of neurons in ANN will also significantly raise the computational cost. In this paper, accurate modeling and relatively fast training are obtained using eight hidden layers with ten neurons in each layer. Once trained, the ANN provides compensation for residual error in the field of view of the OVMS, which models the non-linear behavior and considerable noise.

III. SIMULATION AND EXPERIMENT

A. Simulation Results

Although the OVMS exists for the PPM, the measuring accuracy is determined by the ANN and the image quality captured by the optical sensor. Thus, to verify the robustness and effectiveness of the proposed two-step calibration method, a series of simulations were implemented. These simulations

focused on testing the performances of the proposed method when there were lens distortion, sensor noise in the OVMS and manufacturing error of the calibration object during the calibration process. The OVMS was simulated with distortion and noises based on an open source package [22], and ANN was implemented using the framework Scikit-learn [23]. Moreover, Ridge regression [24] and Lasso method [25] were involved as comparisons to the proposed method.

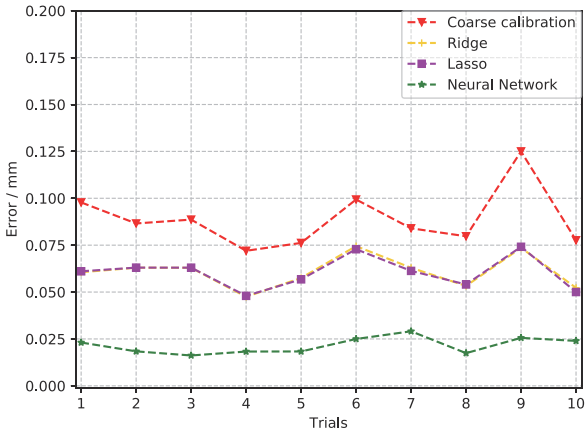

Fig. 3. 10-fold cross validation in simulation, comparing ANN and other methods.

TABLE I

RESULTS TESTED BY SIMULATION

	Position		Orientation	
	Mean	Improvement	Mean	Improvement
Coarse	0.0871 mm	–	0.020°	–
Ridge	0.0543 mm	34.97%	0.0084°	57.91%
Lasso	0.0541 mm	35.20%	0.0095°	52.51%
ANN	0.0195 mm	76.65%	0.0065°	67.44%

The simulation generated 300 training data points within the field of view of the OVMS, then the 10-fold cross validation was firstly performed. The error was calculated by the difference between the true and measured values. Results exhibit in Fig. 3 indicating the proposed method yields the best performances among the four methods in terms of the 10-fold cross validation. ANN not only reduces the most measuring error, but also has a high stability.

Then, the measurement models of the OVMS were calibrated using the training dataset, and these models were tested with a new testing dataset, which contained 100 data points. Table I lists the total simulation results, which indicate that the proposed ANN method has the highest calibration accuracy compared to other three methods. Concretely, the mean absolute measuring error is reduced by 76.65% and 67.44% on position component and orientation component of the OVMS, respectively.

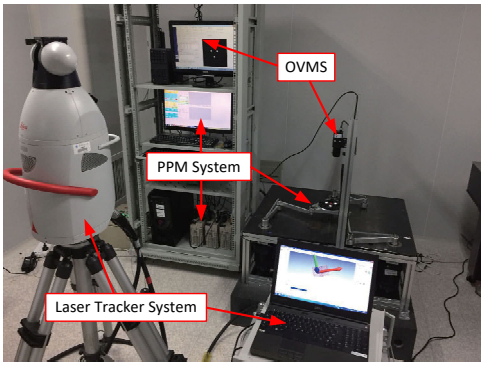

(a)

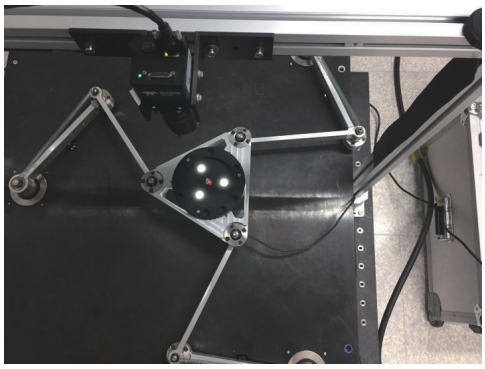

(b)

Fig. 4. The experimental setup. (a) Full view of the setup. (b) Zoom-in picture of the OVMS and the PPM.

B. Experimental Results

The experiments were conducted to validate the proposed two-step calibration in practice application. As presented in Fig. 4, a prototype of the 3-RRR PPM was manufactured and selected as the macro part of our macro-micro manipulator system, as it is the most common architecture with a larger workspace among PPMs [26]. The laser tracker (Leica AT901-B) was employed to calculate the residual error. Connected with the motion control unit of the 3-RRR PPM, the OVMS included an optical lens (Kowa LM16SC), a CMOS sensor (Genie TS M2048), three active markers, and an image acquisition unit inserted inside an image processor. In this OVMS, white LED sources were employed on the back of the marker, so that the measurement accuracy and computational cost can be improved. The basic performance of the image processor was tested in our previous work [27]. The images were captured in the 200 $mm \times 200$ mm field of view by the high-resolution CMOS camera and transmitted to the acquisition unit, and finally processed in an image processor constituted by a high-performance computer.

In the first step, the coarse calibration was performed with a high-precision glass checkerboard, which had $1\mu m$ pattern accuracy. After coarse calibration using Matlab, the theoretical average re-projective error was 0.09 pixel.

In the second step, the fine calibration was conducted to compensate the residual errors. The OVMS and the laser tracker were firstly initialized when the 3-RRR PPM was at

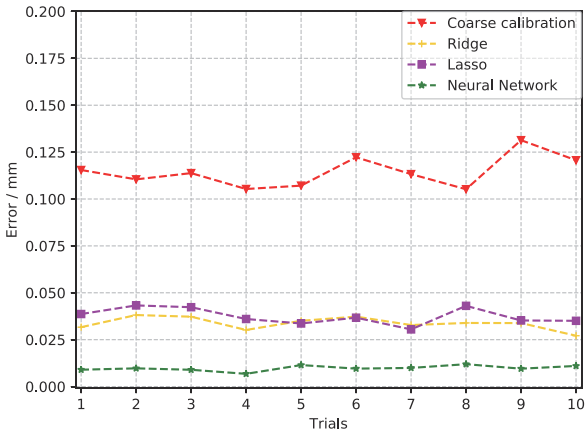

Fig. 5. 10-fold cross validation in experiment, comparing ANN and other methods.

TABLE II

RESULTS TESTED BY EXPERIMENT

	Position		Orientation	
	Mean	Improvement	Mean	Improvement
Coarse	0.1117 mm	–	0.0227°	–
Ridge	0.0316 mm	71.67%	0.0121°	46.99%
Lasso	0.0349 mm	68.76%	0.0125°	44.96%
ANN	0.0093 mm	91.63%	0.0095°	58.00%

the original point. After that, the 3-RRR PPM was moved to each target point within the field of view of OVMS. The post of 3-RRR PPM was measured simultaneously by the OVMS and the laser tracker, and the deviations were regarded as the residual errors. 300 measurements were collected and the residual errors were obtained as the training data. A 10-fold cross validation was then conducted based on this dataset. As can be seen in Fig. 5, the proposed method obtains the highest measuring accuracy and strong robustness with the stablest measurement result, and there is no sign of over-fitting observed.

In order to further evaluate the performance of the proposed method, 100 additional measurements were acquired to test the calibrated OVMS models. The results are listed in Table II. Among all four methods, the proposed method still yields the highest measuring accuracy and gains 91.63% and 58.00% measuring improvement on position and orientation versus the coarse calibration. Compared with Ridge and Lasso approaches in the second step, the proposed method minimized the most measuring errors, which drop from 0.117 mm and 0.0227° to 0.0093 mm and 0.0095°, respectively.

The measuring error distributions using proposed method are visualized in Figs. 6 and 7. It can be seen that, large residual errors mainly distribute around the boundary of the field of view in the coarse calibration. Additionally, the error on orientation shows more randomness than on position, which means the orientation measurement is affected more by non-

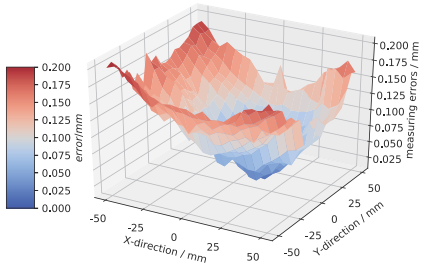

(a)

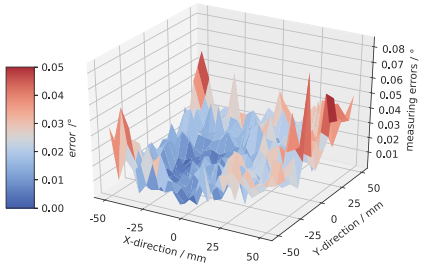

(b)

Fig. 6. Measuring accuracy after coarse calibration with experiment data. (a) Error distribution of position component. (b) Error distribution of orientation component.

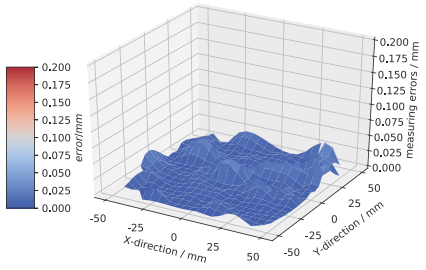

(a)

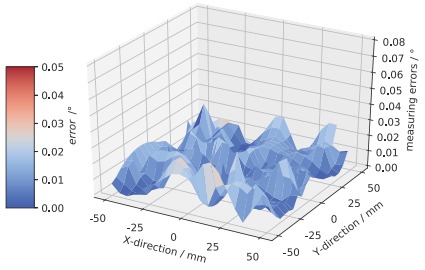

(b)

Fig. 7. Measuring accuracy after fine calibration with experiment data. (a) Error distribution of position component. (b) Error distribution of orientation component.

geometric factors. Using the ANN method, the measuring errors drop remarkably after the fine calibration. Moreover, the peak error value decreases dramatically from $0.2049\ mm$ and $0.0640°$ to $0.0333\ mm$ and $0.02864°$. The error distributions also convert from extremely inhomogeneous to a flat shape, which indicates the proposed two-step method is stable, reliable, and effective.

IV. CONCLUSIONS

In this paper, we present a practical two-step calibration method for vision systems that aim to provide high-precision and strong-robustness measurement for macro-micro manipulation. The proposed calibration method combines the analytic approach and ANN to reduce geometric and non-geometric errors. The OVMS based on the DPnP model is introduced in details, and an ANN is designed for fine calibration. A series of simulations and experiments are performed based on a 3-RRR PPM platform, and the comparisons among the proposed method, single analytic approach, Ridge and Lasso method are discussed. The results show that the proposed method surpasses other methods, and it achieves high measuring accuracy and adaptability in a large field of view. The experimental results also indicate that the calibrated OVMS is stable and suitable for multi-scale measurement, which benefits the study of precision engineering at small scales.

ACKNOWLEDGMENT

REFERENCES

[1] A. Sharon, N. Hogan, and D. E. Hardt, "The macro/micro manipulator: An improved architecture for robot control," *Robotics and computer-integrated manufacturing*, vol. 10, no. 3, pp. 209–222, 1993.

[2] R. Wang and X. Zhang, "Parameters optimization and experiment of a planar parallel 3-dof nanopositioning system," *IEEE Transactions on Industrial Electronics*, vol. PP, no. 99, pp. 1–1, 2017.

[3] S. Yao, H. Li, L. Zeng, and X. Zhang, "Vision-based adaptive control of a 3-rrr parallel positioning system," *Science China Technological Sciences*, vol. 61, no. 8, pp. 1253–1264, 2018.

[4] P. Renaud, N. Andreff, J. M. Lavest, and M. Dhome, "Simplifying the kinematic calibration of parallel mechanisms using vision-based metrology," *IEEE Transactions on Robotics*, vol. 22, no. 1, pp. 12–22, 2006.

[5] S. Levine, C. Finn, T. Darrell, and P. Abbeel, "End-to-end training of deep visuomotor policies," *Journal of Machine Learning Research*, vol. 17, no. 1, pp. 1334–1373, 2016.

[6] Y. Hong, G. Ren, and E. Liu, "Non-iterative method for camera calibration," *Optics Express*, vol. 23, no. 18, pp. 23 992–4003, 2015.

[7] H. Li, X. Zhang, H. Wu, and J. Gan, "Line-based calibration of a micro-vision motion measurement system," *Optics & Lasers in Engineering*, vol. 93, pp. 40–46, 2017.

[8] H. Li, X. Zhang, and B. Zhu, "Single grid image based calibration of an optical microscope," in *2017 International Conference on Manipulation, Automation and Robotics at Small Scales (MARSS)*. IEEE, 2017, pp. 1–6.

[9] R. Klette, A. Koschan, and K. Schluns, *Computer Vision— Three-Dimensional Data from Images*. DBLP, 1998.

[10] C. T. Su, C. A. Chang, and F. C. Tien, *Neural networks for precise measurement in computer vision systems*. Elsevier Science Publishers B. V., 1995.

[11] R. Rojas, *Neural networks: a systematic introduction*. Springer Science & Business Media, 2013.

[12] L. N. Smith and M. L. Smith, "Automatic machine vision calibration using statistical and neural network methods," *Image & Vision Computing*, vol. 23, no. 10, pp. 887–899, 2005.

[13] P. Cerveri, C. Forlani, N. Borghese, and G. Ferrigno, "Distortion correction for x-ray image intensifiers: Local unwarping polynomials and rbf neural networks," *Medical Physics*, vol. 29, no. 8, pp. 1759–1771, 2002.

[14] J.-P. Merlet, "Jacobian, manipulability, condition number, and accuracy of parallel robots," *Journal of Mechanical Design*, vol. 128, no. 1, pp. 199–206, 2006.

[15] S. Yao, X. Zhang, J. Yu, and B. Zhu, "Error modeling and calibration of a 4rrr redundant positioning system," *Aip Advances*, vol. 7, no. 9, p. 095009, 2017.

[16] V. Lepetit, F. Moreno-Noguer, and P. Fua, "Epnp: An accurate o (n) solution to the pnp problem," *International journal of computer vision*, vol. 81, no. 2, p. 155, 2009.

[17] Z. Zhang, "A flexible new technique for camera calibration," *IEEE Transactions on Pattern Analysis and Machine Intelligence*, vol. 22, no. 11, pp. 1330–1334, 2000.

[18] C. M. Bishop, *Pattern Recognition and Machine Learning (Information Science and Statistics)*. Springer-Verlag New York, Inc., 2006.

[19] Y. A. LeCun, L. Bottou, G. B. Orr, and K.-R. Müller, "Efficient backprop," in *Neural networks: Tricks of the trade*. Springer, 2012, pp. 9–48.

[20] A. Krizhevsky, I. Sutskever, and G. E. Hinton, "Imagenet classification with deep convolutional neural networks," in *Advances in neural information processing systems*, 2012, pp. 1097–1105.

[21] Q. V. Le, J. Ngiam, A. Coates, A. Lahiri, B. Prochnow, and A. Y. Ng, "On optimization methods for deep learning," in *Proceedings of the 28th International Conference on International Conference on Machine Learning*. Omnipress, 2011, pp. 265–272.

[22] D. Samper, J. Santolaria, and J. Aguilar, "Metrovisionlab toolbox for camera calibration and simulation," http://metrovisionlab.unizar.es.

[23] F. Pedregosa, A. Gramfort, V. Michel, B. Thirion, O. Grisel, M. Blondel, P. Prettenhofer, R. Weiss, V. Dubourg, and J. Vanderplas, "Scikit-learn: Machine learning in python," *Journal of Machine Learning Research*, vol. 12, no. 10, pp. 2825–2830, 2013.

[24] B. G. Kibria, "Performance of some new ridge regression estimators," *Communications in Statistics-Simulation and Computation*, vol. 32, no. 2, pp. 419–435, 2003.

[25] R. Tibshirani, "Regression shrinkage and selection via the lasso: a retrospective," *Journal of the Royal Statistical Society: Series B (Statistical Methodology)*, vol. 73, no. 3, pp. 273–282, 2011.

[26] I. Bonev and C. M. Gosselin, "Singularity loci of planar parallel manipulators with revolut joints," in *Proceedings of the 2nd Workshop on Computational Kinematics*, 2001, pp. 291—299.

[27] H. Li, X. M. Zhang, L. Zeng, and Y. J. Huang, "A monocular vision system for online pose measurement of a 3rrr planar parallel manipulator," *Journal of Intelligent & Robotic Systems*, no. 2, pp. 1–15, 2017.